Capping Arene Ligated Rhodium Catalyzed Olefin Hydrogenation: A Model Study of the Ligand Influence on a Catalytic Process that Incorporates Oxidative Addition and Reductive Elimination

Ke Zhang[†, #], Charles B. Musgrave III[‡, #], Diane A. Dickie[†], William A. Goddard III[‡*], T. Brent Gunnoe[†*]

[†] Department of Chemistry, University of Virginia, Charlottesville, VA 22904, United States

[‡] Materials and Process Simulation Center, California Institute of Technology, Pasadena, CA 91125, United States

[#] These authors contributed equally

Abstract

The ligand influence on olefin hydrogenation using four capping arene ligated Rh(I) catalyst precursors (FP)Rh(η^2-C_2H_4)Cl {FP = capping arene ligands, including 6-FP (8,8'-(1,2-phenylene)diquinoline), 6-^{NP}FP (8,8'-(2,3-naphthalene)diquinoline), 5-FP (1,2-bis(*N*-7-azaindolyl)benzene) and 5-^{NP}FP [2,3-bis(*N*-7-azaindolyl)naphthalene]} has been studied. Our studies indicate that relative observed rates of catalytic olefin hydrogenation follow the trend (6-FP)Rh(η^2-C_2H_4)Cl > (5-FP)Rh(η^2-C_2H_4)Cl. Based on combined experimental and DFT modeling studies, we propose that the observed differences in rate of (6-FP)Rh(η^2-C_2H_4)Cl and (5-FP)Rh(η^2-C_2H_4)Cl catalyzed olefin hydrogenation are most likely attributed to the difference in the activation energies for the dihydrogen oxidative addition step. We are unable to directly compare the rates of olefin hydrogenation using (6-^{NP}FP)Rh(η^2-C_2H_4)Cl and (5-^{NP}FP)Rh(η^2-C_2H_4)Cl as the catalyst precursor since (5-^{NP}FP)Rh(η^2-C_2H_4)Cl undergoes relatively rapid formation of an active catalyst that does not coordinate 5-^{NP}FP.

Introduction

Many homogeneous catalytic processes based on transition metal catalysts occur through catalytic cycles that form transition metal intermediates in different formal oxidation states. For example, for transition metal-based catalytic processes, oxidative addition and reductive elimination reactions are often key steps in catalytic processes, and these fundamental reactions increase formal metal oxidation state and coordination number (oxidative addition) or decrease formal metal oxidation state and coordination number (reductive elimination).[1-10] A common motif for processes based on group 9 metals is for a catalytic cycle to involve d^8 (+1 oxidation state) and d^6 (+3 oxidation state) intermediates.[7, 11-19] To improve catalytic activity, studies have been directed toward understanding trends for oxidative addition and reductive elimination by tuning a variety of features (e.g., electronic properties of the metal and ligand, steric properties of the ligand).[20-31] Herein, we report on studies to quantify the ability of capping arene ligands to modulate the energetics of Rh-catalyzed olefin hydrogenation by impacting the stability of Rh(I) versus Rh(III) intermediates and transition states.

For catalytic processes that proceed through different transition metal redox states, the different oxidation states present variable d-electron counts and idealized geometries. Ligand design that selectively stabilizes, or destabilizes, a specific redox state, based on d-electron count and/or a preferred geometry/coordination number, potentially can be used to optimize rates of catalysis.[23-25, 32-35] Recently, our group has reported on the use of “capping arene” ligands (FP) with Co, Rh and Ir metals.[27, 35-40] For capping arene-Rh complexes, we have studied the ability of the capping arene structure to modulate the reductive elimination of MeX (X = halides, pseudohalides) from $(FP)Rh^{III}(Me)(X)_2$.[35] The conceptual foundation of our approach is that the structure of different capping arene ligands can control the distance between the metal and an arene group (i.e., the capping arene), and that this controllable metal/arene interaction can be

used to selectively stabilize or destabilize intermediates and/or transition states. Thus, this approach is different from approaches such as hemilabile ligands, which can facilitate catalysis through dissociation/re-coordination of a coordinating group. Having observed differences in these stoichiometric reactions based on capping arene ligand identity, we sought to extend our studies and understanding of the impact of capping arene ligands using a well understood catalytic reaction.

In this work, we sought a reaction with a well-defined set of possible mechanistic pathways and clear involvement of M^n and M^{n+2} formal oxidation states that are formed via oxidative addition and reductive elimination reactions. Thus, Rh-catalyzed olefin hydrogenation was selected for the model study. Although specific mechanisms may vary based on ligand(s), olefin substrate, and conditions, the key steps of olefin hydrogenation are usually proposed to be oxidative addition of H_2, olefin coordination, migratory insertion of coordinated olefin into a Rh-hydride bond, and reductive elimination from a Rh^{III}(H)(alkyl) intermediate to release the hydrogenated product (Scheme 1).[6, 17, 41-50] Previous studies have shown that the oxidative addition is often the rate-determining step for Rh(I) catalyzed olefin hydrogenation.[6, 42-46] Thus, we anticipated that the capping arene ligated Rh(I) catalyzed olefin hydrogenation would follow one of the general mechanisms shown in Scheme 1, during which the oxidative addition of H_2 on the Rh(I) metal center would likely play an important role in the catalytic cycle.

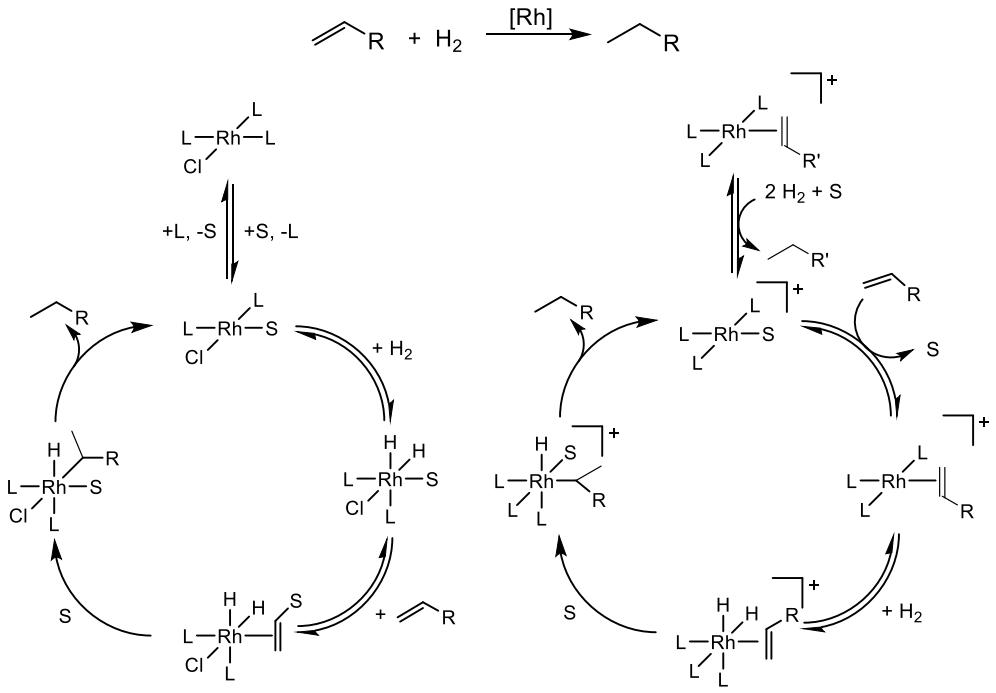

S = solvent; L = ligand

Scheme 1. General mechanisms for homogenous Rh-catalyzed olefin hydrogenation reactions.

Herein, we report on studies of capping arene ligated Rh(I) catalyzed olefin hydrogenation including combined experimental and computational studies to understand the mechanism and quantify catalytic performance. Our studies reveal that the reaction rate of olefin hydrogenation is dependent on the capping arene ligands on Rh, for which the trend is identified to be (6-FP)Rh(η^2-C_2H_4)Cl > (5-FP)Rh(η^2-C_2H_4)Cl (Scheme 2). Combined experimental and computational modeling studies allow us to understand and explain the relative rates of reaction based on the identity of the Rh catalyst precursor. Catalytic olefin hydrogenation using (5-^{NP}FP)Rh(η^2-C_2H_4)Cl and (6-^{NP}FP)Rh(η^2-C_2H_4)Cl was also studied; however, under conditions of catalysis, the complex (5-^{NP}FP)Rh(η^2-C_2H_4)Cl likely forms an active catalyst that is not ligated by the 5-^{NP}FP ligand, and thus comparison of catalysis using (5-^{NP}FP)Rh(η^2-C_2H_4)Cl versus (6-^{NP}FP)Rh(η^2-C_2H_4)Cl was not possible.

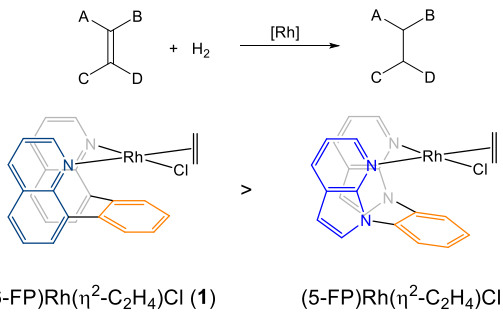

Scheme 2. Trend of ligand impact on rate of catalytic olefin hydrogenation using capping arene ligated Rh complexes as catalyst precursors.

Result and Discussion

We studied four capping arene Rh(I) complexes as catalyst precursors for olefin hydrogenation of the general formula (capping arene)Rh(η^2-C_2H_4)Cl. The capping arene ligands that we studied include 6-FP (8,8′-(1,2-phenylene)diquinoline, **1** in Scheme 3), 5-FP (1,2-bis(*N*-7-azaindolyl)benzene, **2** in Scheme 3), 6-^{NP}FP (8,8′-(2,3-naphthalene)diquinoline, **3** in Scheme 3), and 5-^{NP}FP (2,3-bis(N-7-azaindolyl)naphthalene, **4** in Scheme 3). Our previous studies indicated that the arene groups (benzene for FP, and naphthalene for ^{NP}FP) can coordinate to the Rh center in a dihapto fashion, and the quinolinyl or *N*-7-azaindolyl backbones can be used to tune the coordination of the arene based on the structure and position of the arene moiety.[35, 38] Structures based on single-crystal X-ray diffraction data show that the distances from Rh center to the closest carbon(s) on the arene moiety are shorter in **1** than in **2** (~2.6 Å vs. ~3.1 Å).[35] This structural difference could influence the relative stabilities of Rh(I) complexes, which often favors a square planar structure, versus Rh(III), which often favors an octahedral structure. Thus, we anticipated that the relative rates of catalytic olefin hydrogenation would depend on the identity of the capping arene ligand.

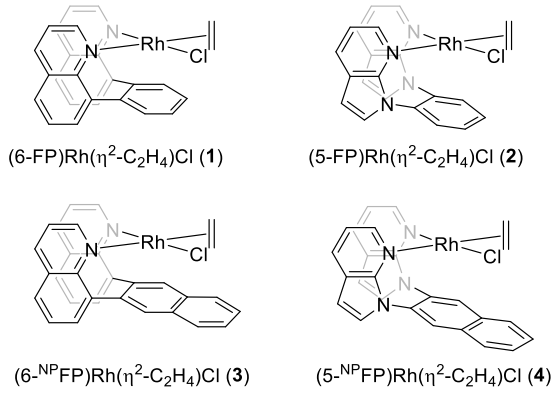

Scheme 3. Examples of (capping arene)Rh(η^2-C_2H_4)Cl complexes used in this study.

The preparation of capping arene-Rh complexes in this study followed previously reported methods.[35] We compared Rh-catalyzed hydrogenation of various olefins (Figure 1) by monitoring catalysis *in situ* using ^{1}H NMR spectroscopy. In a representative experiment, a J. Young tube was charged with 0.4 mL of a 1 mM solution of Rh complex, 4 mM of hexamethylbenzene (HMB, internal standard), and 44 mM of olefin in CD_2Cl_2 followed by pressurizing with 50 psig of H_2. The reaction tube was heated to 45 °C, and ^{1}H NMR spectra were collected at 0, 1, 2 and 4 hours. The concentration of olefin, hydrogen and the hydrogenated product were determined by the integration with respect to the internal standard HMB. For the hydrogenation of cyclohexene, styrene, *trans*-2-pentene and *cis*-2-pentene (Figure 1), the reaction rate data show that the rate of hydrogenation using either **1** or **3** is faster than **2**. The catalyst precursor **4** gives the most rapid catalysis, but we have evidence that **4** converts to a catalyst that is not ligated by the 5-^{NP}FP ligand (see below for more details). Thus, we have excluded data for **4** from Figure 1. In comparison, the rates for hydrogenation of 3,3-dimethyl-1-butene with the three catalysts do not show a statistically significant difference. The hydrogenation of tri-substituted and tetra-substituted olefins 2-methyl-2-butene and 2,3-dimethyl-butene does not occur with any of the Rh catalysts. Also, the hydrogenation of *trans*-stilbene was not observed.

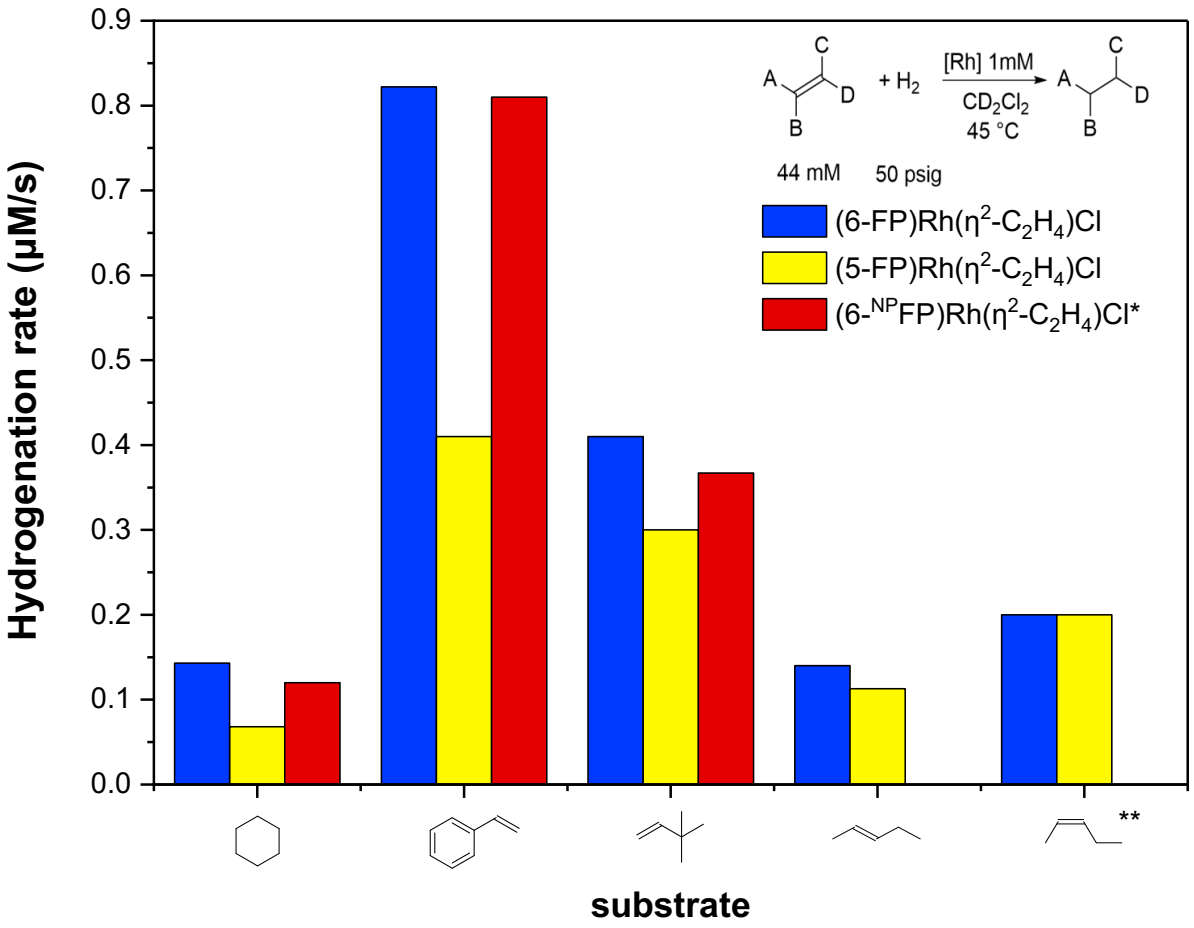

Figure 1. Comparison of olefin hydrogenation rate with various olefin using catalyzed by (FP)Rh(η^2-C_2H_4)Cl (FP = 5-FP, 6-FP or 6-^{NP}FP). The bars show rate data from at least three independent experiments with standard deviations shown as error bars. * Complex **3** is not stable at prolonged reaction times. Thus, the rate data were determined using data collected at 0, 20, 40 and 60 minutes. ** The isomerization of *cis*-2-pentene to *trans*-2-pentene and 1-pentene competes with the hydrogenation of *cis*-2-pentene. Thus, the rate of catalytic hydrogenation of *cis*-2-pentene could not be accurately quantified.

Overview of possible catalytic mechanism. To understand the trend of the ligand effect shown in Figure 1, a series of mechanistic studies were performed. Scheme 4 shows two mechanisms for catalytic olefin hydrogenation using (FP)Rh(η^2-C_2H_4)Cl based on the general mechanisms of Rh catalyzed olefin hydrogenation shown in Scheme 1.[6, 17, 42, 50] The proposed mechanism on the left (Scheme 4A) is the "olefin first" mechanism. In this mechanism, the precursor (FP)Rh^{I}(η^2-C_2H_4)Cl first undergoes olefin exchange to form (FP)Rh^{I}(η^2-olefin)Cl (Step **a**). Then, oxidative addition of H_2 takes place to generate the cationic Rh(III) complex

$[(FP)Rh^{III}(H)_2(\eta^2\text{-olefin})]^+$ with an outer sphere chloride anion (Step **b**). After that, olefin migratory insertion leads to the formation of $[(FP)Rh^{III}(H)(\kappa^1\text{-hydrocarbyl})]Cl$ (Step **c**). Finally, the hydrogenated product is released by reductive elimination, and the Rh complex coordinates another equivalent of olefin to form $(FP)Rh^{I}(\eta^2\text{-olefin})Cl$ (Step **d**). The proposed mechanism on the right (Scheme 4B) is the "hydrogen first" mechanism. In this mechanism, $(FP)Rh^{I}(\eta^2\text{-}C_2H_4)Cl$ reacts with H_2 first to give the oxidative addition product (Step **e**), followed by olefin exchange to form $[(FP)Rh^{III}(H)_2(\eta^2\text{-olefin})]Cl$ (Step **f**). The catalytic cycle starting with $[(FP)Rh^{III}(H)_2(\eta^2\text{-olefin})]Cl$ is similar to the cycle in Scheme 4A, which undergoes an olefin migratory insertion (Step **g**), reductive elimination and olefin coordination (Step **h**), and H_2 oxidative addition (Step **i**).

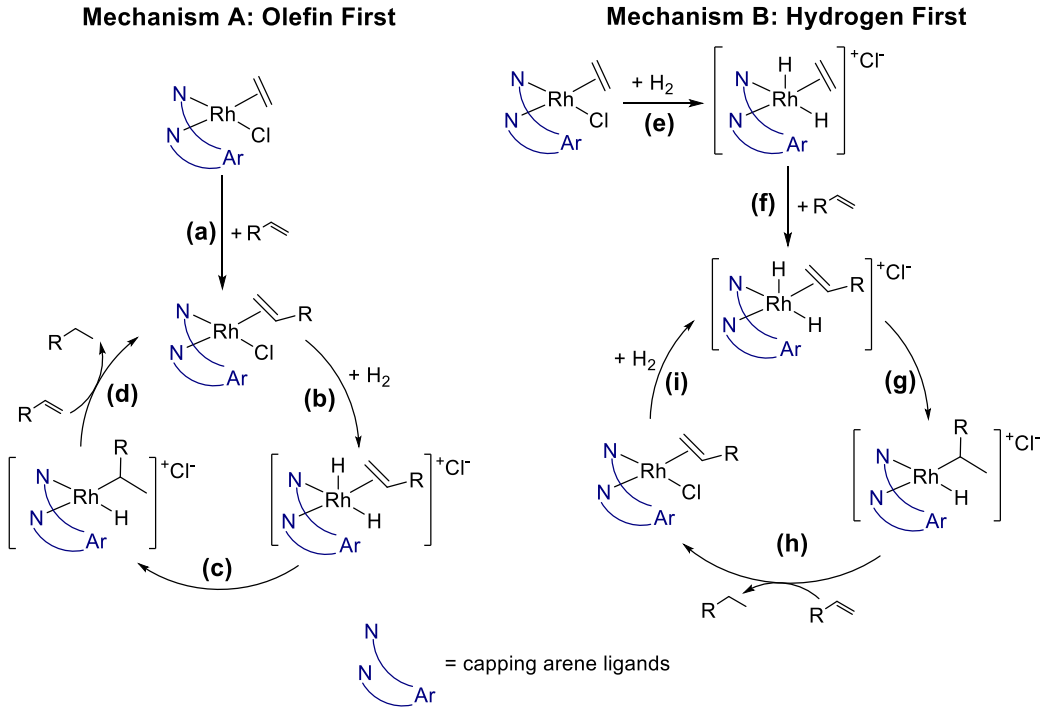

Scheme 4. Two proposed mechanisms for FP-Rh catalyzed olefin hydrogenation.

Kinetic studies. To further understand the mechanism of the FP-Rh catalyzed olefin hydrogenation, we studied the dependence of reaction rate on dihydrogen pressure using **1** and styrene using the method of initial rates. The initial concentration of dihydrogen in solution phase

was determined by the integration of the resonance due to dissolved H_2 compared to the internal standard HMB. A plot of ln(k_{obs}) versus ln[H_2] (Figure 2A) shows a slope close to 1, indicating the reaction likely has a first order dependence on dihydrogen concentration. The plot of ln(k_{obs}) versus ln[**1**] (Figure 2B) shows a slope of 0.95(4), indicating a likely first order dependence on the concentration of **1**. A plot of k_{obs} vs. [styrene] with a curve fit using the function y = ax / (b + x) in Figure 2C shows an R^2 value of 0.95, indicating a Michaelis–Menten relationship (a = V_{max}, b = K_M). One possible explanation for the Michaelis–Menten relationship based on concentration of styrene is a reversible exchange of ethylene between **1** and styrene prior to the H_2 oxidative addition.[51] When the styrene hydrogenation is performed with a substantial excess of styrene, which is calculated to be 0.9(4) mol/L for the experimental condition (see Supporting Information), the styrene exchange becomes the fast step, which would lead to a zero-order rate law in styrene.[51] Based on these studies, a rate equation for the **1** catalyzed styrene hydrogenation is shown in Eq. 1. When styrene concentration is significant, the rate equation can be expressed by Eq. 2.

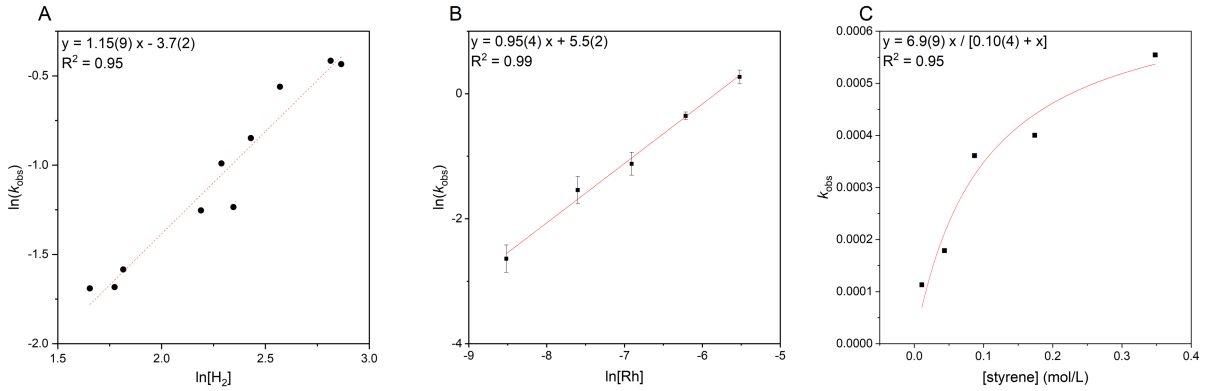

Figure 2. Studies of reaction order for hydrogenation of styrene using (6-FP)Rh(Cl)(η^2-C_2H_4) (**1**). The reaction conditions are: For the determination of order in H_2 (Figure 2A): 1 mM **1**, 44 mM styrene, variable psig of H_2 (20, 30, 40 or 50 psig), 45 °C. For the determination of order in **1** (Figure 2B): variable mM **1** (0.2, 0.5, 1, 2 or 4 mM), 44 mM styrene, 50 psig H_2, 45 °C. For the determination of order in styrene (Figure 2C): 0.5 mM **1**, variable mM styrene (11, 44, 87, 174 or 348 mM), 50 psig H_2, 45 °C.

$$\text{rate} = k[\mathbf{1}][H_2][\text{styrene}] \qquad (1)$$

$$\text{rate} = k'[\mathbf{1}][H_2] \qquad (2)$$

In the Supporting Information, we show the rates of olefin hydrogenation using **4** as the catalyst precursor. In all cases, catalysis with **4** is substantially faster than the other capping arene Rh complexes. The rate dependences on $[H_2]$ and [Rh] for the **4** catalyzed styrene hydrogenation was determined. Similar to 6FP-A catalyzed styrene hydrogenation, a first order dependence on $[H_2]$ was observed (Figure 3A). However, surprisingly, the results in Figure 3B suggests a half-order dependence on concentration of **4**. This half-order dependence on [**4**] suggests the possible formation of a dimeric Rh complex from **4**.[52, 53] For example, dissociation of the 5-^{NP}FP ligand could form a chloride-bridged Rh dimer, which could serve as the catalyst precursor (see Supporting Information Section 6.3 for details). Consistent with this hypothesis, the rate dependence on [Rh] using $[Rh(\eta^2\text{-}C_2H_4)_2(\mu\text{-}Cl)]_2$ as the catalyst precursor for styrene hydrogenation revealed a half-order dependence (Figure 3C), and the observed rate is at least 10 times faster than the **4** catalyzed styrene hydrogenation under the same conditions. Although the active species in **4** catalyzed styrene hydrogenation could be different from the active species for $[Rh(\eta^2\text{-}C_2H_4)_2(\mu\text{-}Cl)]_2$, the difference in rate law on [**4**] and [**1**] for their catalytic styrene hydrogenation is evidence that the catalytic styrene hydrogenation for **4** and **1** undergoes different mechanisms, in which **4** is likely to form a dimeric species without the 5-^{NP}FP ligand during the catalysis, while the active catalyst for **1** maintains the monomeric form during catalysis.

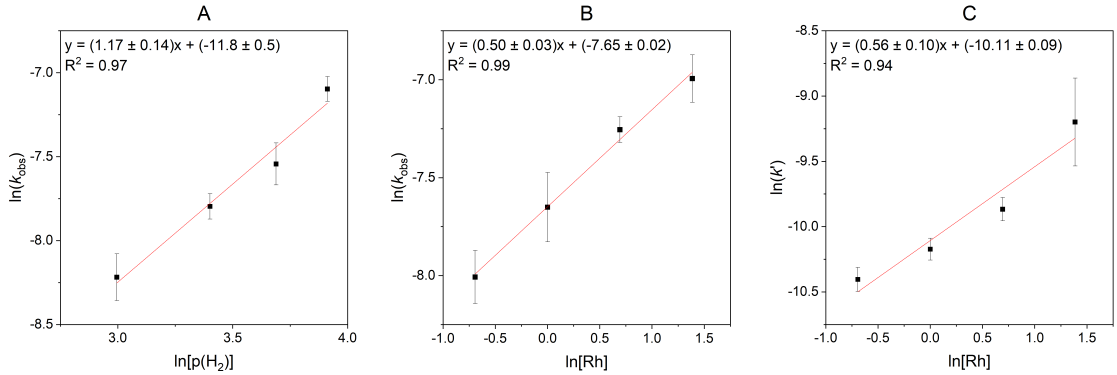

Figure 3. Studies of reaction order for hydrogenation of styrene using (5-^{NP}FP)Rh(Cl)(η^2-C_2H_4) (**4**) or [Rh(η^2-C_2H_4)(μ-Cl)]$_2$. The reaction conditions are: For the determination of order in H_2 (Figure 3A): 1 mM **4**, 87 mM styrene, variable psig of H_2 (20, 30, 40 or 50 psig), 45 °C. For the determination of order in **4** (Figure 3B): variable mM **4** (0.5, 1, 1.5, 2 or 4 mM), 87 mM styrene, 50 psig H_2, 45 °C. For the determination of order in [Rh(η^2-C_2H_4)(μ-Cl)]$_2$ (Figure 3C): variable mM **4** (0.25, 0.5, 0.75, 1 or 2 mM), 44 mM styrene, 50 psig H_2, 45 °C.

To estimate the activation energy for our Rh-catalyzed styrene hydrogenation, an Eyring analysis was performed by measuring the reaction rate at temperatures from 25 °C to 55 °C. The resulting Eyring plot shows a linear fit with $R^2 > 0.95$. The $\Delta H^{\ddagger}$ and $\Delta S^{\ddagger}$ values were calculated to be 12.6(9) kcal/mol and -23(3) cal/K·mol, respectively (Figure 4). The negative value of activation entropy ($\Delta S^{\ddagger}$) is similar to the $\Delta S^{\ddagger}$ for styrene hydrogenation catalyzed by Wilkinson's catalyst (-21.5 cal/K·mol).[54]

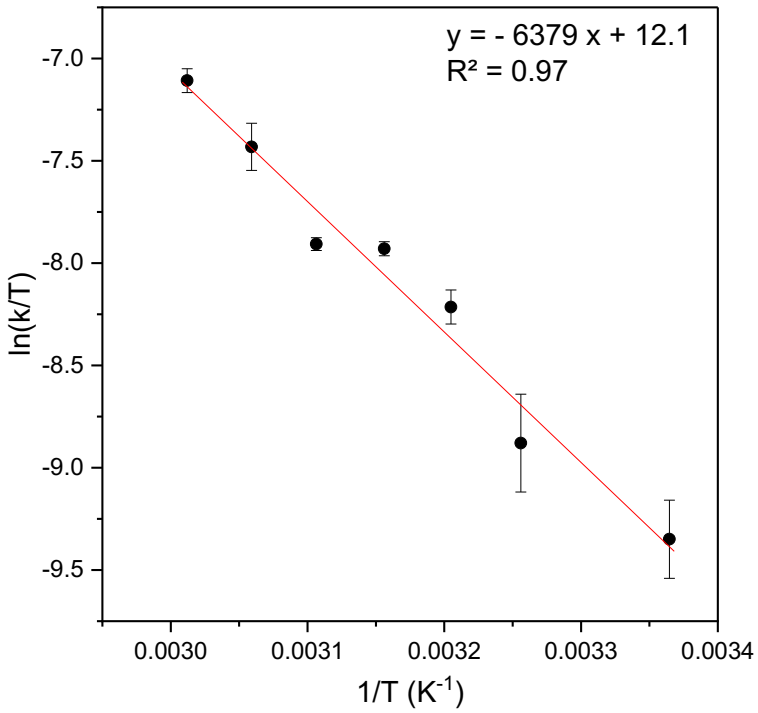

Figure 4. Eyring plot for the hydrogenation of styrene catalyzed by (6-FP)Rh(η^2-C_2H_4)Cl (**1**). All data points and standard deviations are based on at least three independent experiments. Reaction conditions: 1 mM **1**, 44 mM styrene, 50 psig H_2, variable temperature (24, 34, 39, 43, 4 , 54 or 59 °C).

Observation and characterization of (6-FP)Rh(Cl)(η^2-styrene). While monitoring styrene hydrogenation using **1** as catalyst precursor by ^{1}H NMR spectroscopy, new resonances in the aromatic region were observed, which are likely due to the active catalyst or an intermediate for the Rh catalyzed styrene hydrogenation. To study the identity of this new Rh complex, styrene and **1** were mixed in CD_2Cl_2, which leads to the formation of (6-FP)Rh(Cl)(η^2-styrene) (**1a**). Since the new aromatic resonances in the ^{1}H NMR spectrum of styrene hydrogenation catalyzed by **1** are consistent with the chemical shifts of the isolated **1a** formed by olefin exchange, we propose that the first step of this styrene hydrogenation reaction is likely to be the formation of **1a**. The ^{1}H NMR spectrum of isolated **1a** shows two sets of resonances with an integration ratio of ~1:1.5. This ratio does not show a detectable change at different concentrations of **1a**. Exchange peaks

between the two species observed by ^{1}H NMR spectroscopy were observed by a 2D-Exchange Spectroscopy (2D-EXSY) experiment, which indicates that the two species likely undergo exchange (Figure S64 in Supporting Information). The rate constant for the exchange between the two species was determined to be 0.076 s^{-1} (see details for the calculation in Supporting Information). Coalescence or line broadening of the two species is not observed by raising the temperature of the NMR probe up to 70 °C. Instead, decomposition of **1a** is observed at 70 °C.

It is established that the generally preferred olefin orientation in square planar and d^8 complexes is with the C=C bond perpendicular to the square plane;[40, 55, 56] however, the capping arene ligand of **1a** can potentially be considered a tridentate ligand, which complicates consideration of the coordination environment around Rh including olefin orientation and rotational dynamics (Figure 5).[38] A single crystal X-ray diffraction study of **1a** indicates that the 6FP capping arene ligand serves as a tridentate ligand, coordinating to the Rh center with two quinoline nitrogen atoms (N1, N2) and the benzene ring in η^2 fashion (C10 and C11) (Figure 6). The geometry of **1a** is approximately trigonal bipyramidal, in which the triangular plane consists of one of the quinoline nitrogen (N1), arene moiety on the ligand (C10 and C11) and the styrene (C25 and C26), and the axial positions are coordinated to the second quinoline nitrogen (N2) and the chloride (Cl1). The bond angles are slightly distorted from the ideal trigonal bipyramidal geometry. The bond angle between N1 and the centroid of C10 and C11 is 88.1°. The angles between the centroid of the styrene C=C bond and N1 or centroid of C10 and C11 are 137.2° and 133.7°, respectively. The styrene C=C bond is oriented in the trigonal plane with a slight distortion (the dihedral angle between the plane of N1–Rh1–C10–C11 and the plane of N1–Rh1–C25–C26 is 6.01°). The bond lengths between Rh center and ligated atoms do not exhibit a significant difference from the corresponding bond lengths in **1** (≥ 0.04 Å).[23] Interestingly, although the DFT calculations on the structure of **1a** in the solid-state is consistent with the crystal structure, DFT

calculations suggest a square planar conformation with the arene moiety at the axial position of the plane when **1a** is dissolved in dichloromethane. One explanation for the preference of trigonal bipyramidal conformation for **1a** in the solid phase is that the π-π stacking between the phenyl ring of coordinated styrene and the quinoline ring with N2 (the distance between the centroids of these two rings is 3.484 Å) could stabilize the trigonal bipyramidal conformation.

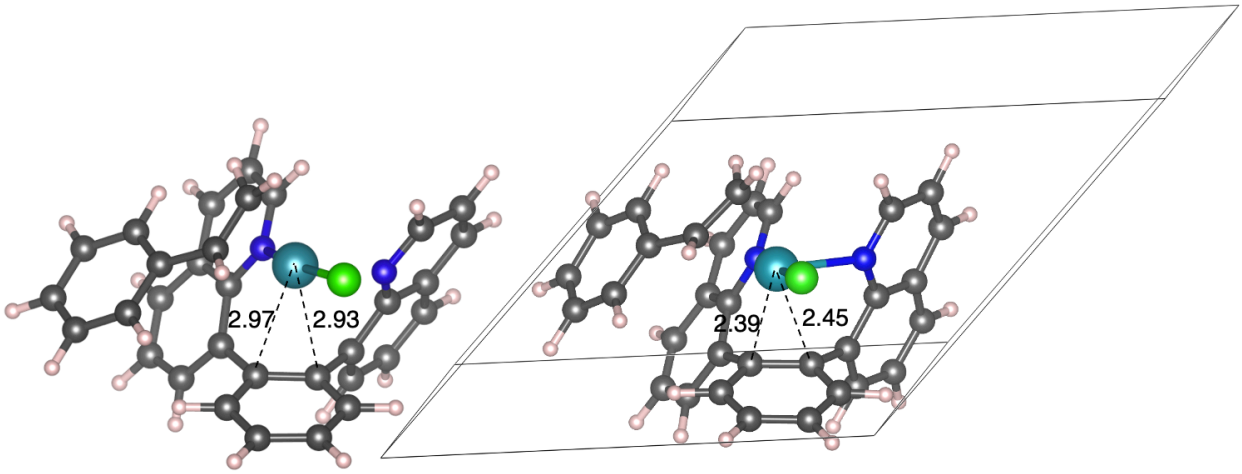

Figure 5. DFT calculated structure of (6-FP)Rh(Cl)(η^2-styrene) (**1a**). The left structure is calculated using solvent parameters with dielectric constant = 8.93 and probe radius = 2.33 Å to match dichloromethane. The right structure is calculated using crystal optimization.

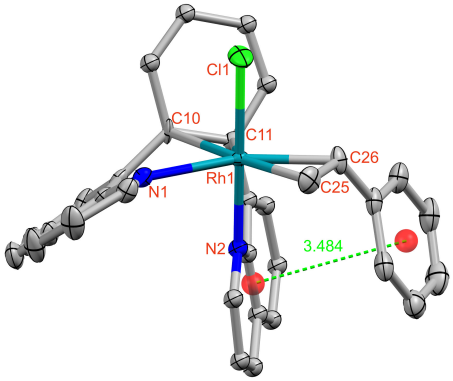

Figure 6. ORTEP of (6-FP)Rh(Cl)(η^2-styrene) (**1a**). Ellipsoids are drawn at 50% probability level. Hydrogen atoms and noncoordinating solvents are omitted for clarity. Selected bond lengths for **1a** (Å): Rh1-N1 2.188(4), Rh1-N2 2.093(10), Rh1-Cl1 2.3448(12), Rh1-C10 2.541(5), Rh1-C11 2.522(16), Rh1-C25 2.060(5), Rh1-C26 2.122(5), C25-C26 1.420(8). Selected bond angles for **1a** (deg): Cl1-Rh1-N1 94.08(10), Cl1-Rh1-N2 178.4(3), Cl1-Rh1-C10 95.98(12), Cl1-Rh1-C11 104.0(3), Cl1-Rh1-C25 87.08(16), Cl1-Rh1-

C26 88.88(15), N1-Rh1-N2 86.2(3), N1-Rh1-C10 71.86(16), N1-Rh1-C11 104.6(3), N1-Rh1-C25 117.2(2), N2-Rh1-C10 83.6(3), N2-Rh1-C11 74.4(4), N2-Rh1-C25 94.2(3), N2-Rh1-C26 91.5(4), The distance between the centroid of the phenyl ring of coordinated styrene and the centroid of the quinoline ring containing N2 is 3.484 Å.

The observation of exchange peaks in the ^{1}H NMR spectrum of **1a** are attributed to dynamics of the C=C bond of styrene. Assuming a preferred C=C orientation in the square plane of the approximately square planar structure (see above and Figure 5), four styrene isomers are possible (Scheme 5). The four isomers can undergo exchange by either rotation of the styrene C=C bond or face flipping (either with or without styrene dissociation).[57-61] The observation of two isomers by ^{1}H NMR spectroscopy indicates that the conformational changes are likely slow on the NMR timescale and that two isomers are likely thermodynamically favored. The thermodynamics of these conformers were probed with DFT (Scheme 5). DFT predicts the LC (lower-cis, cis relative to the 6FP backbone) conformation to be the lowest in Gibbs free energy due to favorable van der Waals (vdW) interactions between the aryl ring of styrene and the capping arene. At 318 K, the UC (upper-cis) conformation lies 1.5 kcal/mol above the LC conformer according to DFT. UC also benefits from favorable vdW interactions with the 6FP moiety, although here the π-π stacking is poorly aligned such that UC is not stabilized as much as LC. The UT (upper-trans) and the LT (lower-trans) structures reside 4.71 and 4.74 kcal/mol above the LC configuration. Neither of these conformers exhibit vdW stabilizing interactions between styrene and the capping arene. Thus, the DFT calculations predict that the two experimentally observed species are LC (major) and UC (minor).

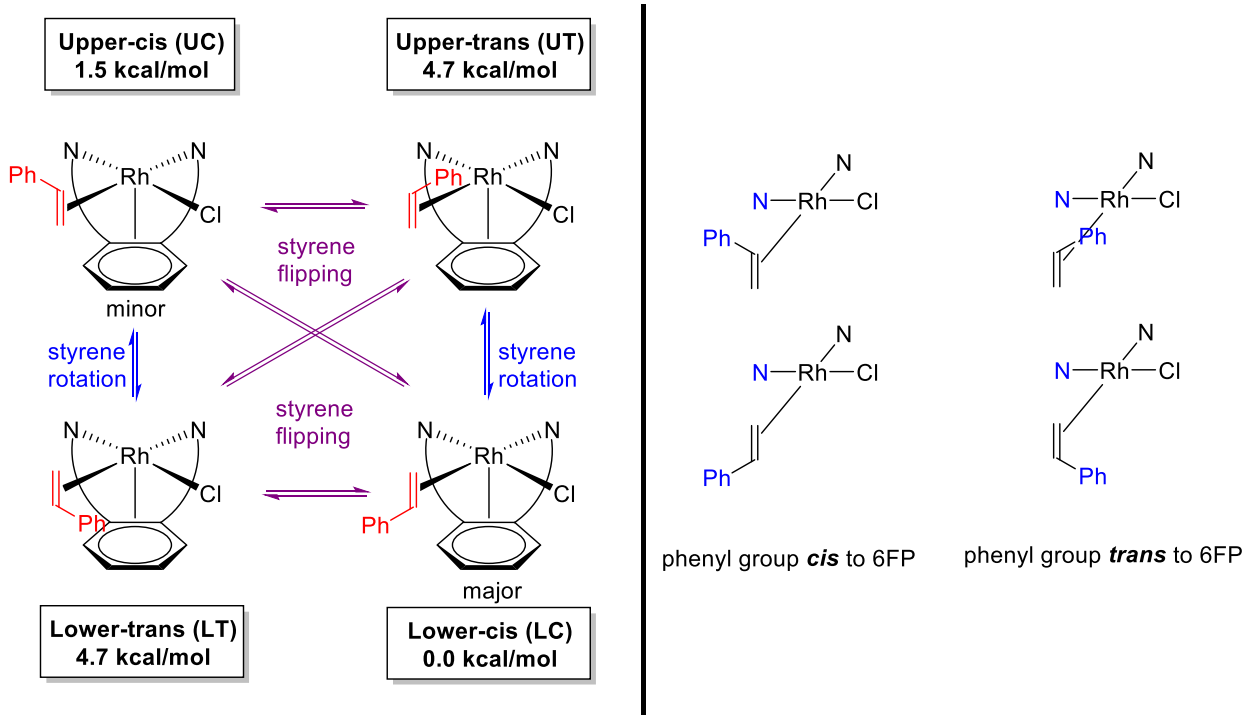

Scheme 5. Possible conformational isomers of (6-FP)Rh(Cl)(η²-styrene) (**1a**) and proposed exchange pathways. The conformers' short-hand names and DFT free energies at 318 K are boxed; U (upper) indicates the phenyl group of styrene points to the opposite position of the arene moiety of the 6FP ligand, L (lower) indicates the phenyl group of styrene points towards the arene moiety of the 6-FP ligand, C indicates *cis* to the 6-FP ligand backbone, T indicates *trans* to the 6-FP ligand backbone, which is illustrated on the right of Scheme 5.

Isotopic scrambling between styrene and D_2. A study using D_2 and styrene was performed to further explore the catalytic styrene hydrogenation. The result of this isotopic study indicates that deuterium is incorporated into ethylbenzene more selectively in the terminal methyl position of the ethyl group (Scheme 6). For a catalytic process that involves irreversible oxidative addition of H_2 (or D_2), it is expected that D will be equally incorporated into the benzylic and methyl positions of ethylbenzene.[62] Monitoring the conversion of styrene and D_2 to ethylbenzene using **1** as catalyst precursor reveals that the benzylic position of ethylbenzene contains 0.54(3) ^{2}D and 1.46(3) ^{1}H (or 27% deuterated), and the methyl position of ethylbenzene contains 1.38(6) ^{2}D and 1.62 (6) ^{1}H (or 46% deuterated). Hence, the hydrogenation process likely involves reversible activation of H_2 and irreversible ethylbenzene formation because the distribution of D on

ethylbenzene would be equivalent at both the benzylic and methyl positions if an irreversible H_2 oxidative addition pathway is followed. Further, isotopic scrambling between styrene and D_2 was observed. After 48 hours of reaction with the conditions indicated in Scheme 6, the product of H/D exchange was observed by ^{1}H NMR spectroscopy (Figure 7). The major H/D exchange products for styrene are the terminal substituted products, *trans*-1-deutero-styrene (6.74 ppm, $^3J_{HH}$ = 11 Hz; 5.25 ppm, *d*, $^3J_{HH}$ = 11 Hz) and *cis*-1-deutero-styrene (6.75 ppm, *d*, $^3J_{HH}$ = 18 Hz; 5.77 ppm, *d*, $^3J_{HH}$ = 18 Hz). Additionally, resonances for free HD (4.59 ppm, *t*, $^1J_{HD}$ = 43 Hz) and H_2 (4.59 ppm, *s*) are observed, which can be attributed to the H/D exchange between styrene and D_2. Thus, the observation of isotopic scrambling between styrene and D_2 provides evidence that the activation of styrene and dihydrogen are likely both reversible.

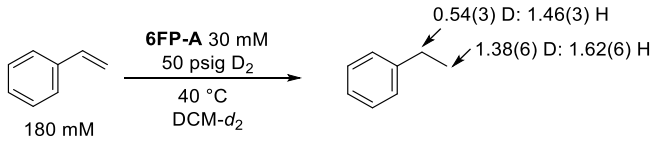

Scheme 6. Isotopic study for (6-FP)Rh(Cl)(η^2-C_2H_4) (**1**) catalyzed styrene hydrogenation. The reaction is performed in triplicate with following conditions: 0.5 mL CD_2Cl_2, 180 mM styrene, 30 mM **1**, 50 psig D_2, 40 °C. The reaction is monitored by ^{1}H NMR spectroscopy every 24 hours. The data for deuterium incorporation are after 48 hours of reaction.

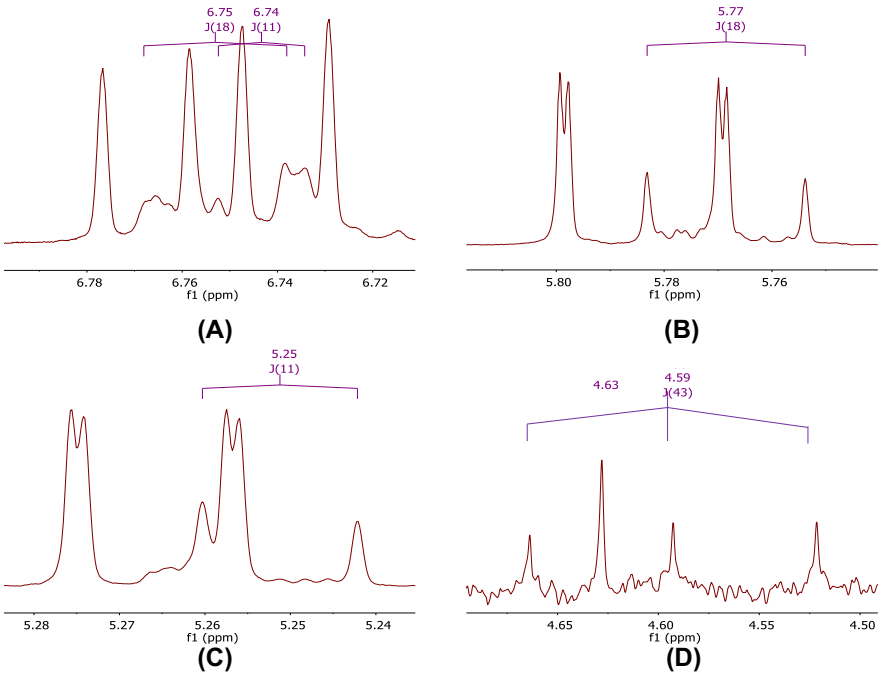

Figure 7. ^{1}H NMR spectroscopy evidence for H/D exchange between styrene and D_2. (A), (B), (C): the three vinyl peaks for styrene. (D): the HD and H_2 peaks. The reaction was performed in triplicate with the following conditions: 0.5 mM CD_2Cl_2, 180 mM styrene, 30 mM (6-FP)Rh(Cl)(η^2-C_2H_4) (**1**), 50 psig D_2, 40 °C. The reaction was monitored by ^{1}H NMR spectroscopy every 24 hours. The data for deuterium incorporation correspond to 48 hours of reaction.

Based on our experimental studies, a mechanism for the styrene hydrogenation process using **1a** as catalyst precursor is proposed (Scheme 7). The oxidative addition of D_2 (or H_2) to **1a** forms [(6-FP)Rh(D)$_2$(η^2-styrene)]Cl (**1b-*d*$_2$**), and **1b-*d*$_2$** can mediate migratory insertion of styrene into a Rh–D bond to form [(6-FP)Rh(D)(1-phenyl-2-D-ethyl)]Cl or [(6-FP)Rh(D)(1-D-2-phenylethyl)]Cl (**1c-*d*$_2$** or **1c'-*d*$_2$**). The reverse reaction, β-hydride elimination, can form [(6-FP)Rh(H)(D)(η^2-styrene-*d*$_1$)]Cl (**1b'-*d*$_2$**), which can undergo ligand exchange with free styrene to generate free styrene-*d*$_1$ and [(6-FP)Rh(H)(D)(η^2-styrene)]Cl (**1b-*d*$_1$**). Net H–D reductive elimination of [(6-FP)Rh(H)(D)(η^2-styrene)]Cl can occur to form the observed formation of free HD. The formation of dihydrogen (H_2) is likely generated from H/D exchange between HD and styrene via the same pathway. Moreover, the observation of the terminal exchange product (C_6H_5–CH=CHD) can be explained by the favored formation of the branched olefin insertion product [(6-FP)Rh(D)(1-

phenyl-2-D-ethyl)]Cl (**1c'-*d*$_2$**) rather than the olefin insertion product [(6-FP)Rh(D)(1-D-2-phenylethyl)]Cl (**1c-*d*$_2$**).

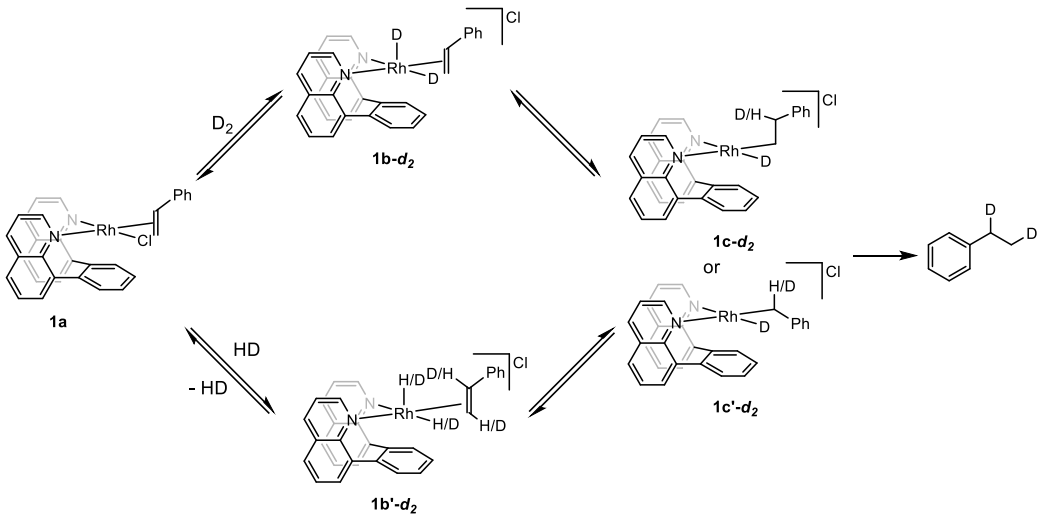

Scheme 7. Proposed mechanism that explains deuterium incorporation into ethylbenzene during styrene hydrogenation using (6-FP)Rh(Cl)(η^2-C_2H_4) (**1**) as catalyst precursor and D_2.

Mechanistic Studies based on Density Functional Theory. To understand how the capping arene ligand identity influences the Rh-catalyzed hydrogenation of olefins, we performed Density Functional Theory (DFT) calculations. These calculations utilized the B3LYP functional with the D3 correction for London dispersion (van der Waals attraction) forces.

The mechanism we studied, based on experimental results (see above), begins with displacement of a coordinated ligand with the olefin to be hydrogenated. The metal catalyst then undergoes oxidative addition by H_2 to generate two hydride ligands. With two hydrides and the olefin present, the olefin then undergoes insertion into an [M]–H bond (M = metal) to form an alkyl ligand. Finally, the catalyst reductively eliminates the second hydride to form the alkane.

Starting with (5-FP)Rh(η^2-C_2H_4)Cl (**2**), displacement of ethylene with styrene is uphill by 3.7 kcal/mol. As expected, styrene prefers to bind the Rh via the alkenyl chain as opposed to the

phenyl ring (see Supporting Information). The DFT calculations predict little geometric change between Rh and the capping arene when ethylene and styrene are exchanged. The Rh–C_{cap} distances for **2** are calculated to be 3.14 Å and 3.16 Å; whereas when styrene is coordinated these distances are both calculated to be 3.12 Å. With the formation of (5-FP)Rh(η^2-styrene)Cl (**2a**), the complex can now dissociate chloride and undergo subsequent H_2 oxidative addition towards [(5-FP)Rh$(H)_2$(η^2-styrene)]Cl (**2b**). The oxidative addition transition state (**2-TS1**) lies 21.0 kcal/mol above the starting state. In **2-TS1**, one of the H atoms from H_2 maintains a non-covalent interaction with the nearby chloride, leading to unequal Rh–H distances: one Rh–H distance is 1.53 Å while the other is 1.67 Å (the former H being in-plane with the N-Rh-N and the latter being the axial H directed towards Cl^-). Additionally, in **2-TS1**, the C=C bond of styrene orients parallel to the N–Rh–N plane (Figure 8), despite the preferred orthogonal orientation in **2a**. Following oxidative addition of dihydrogen, the free energy of **2b** lies 16.0 kcal/mol above the starting state; this high free energy confirms the bias towards Rh(I) when bound to the capping arene ligand.

The complex **2b** can undergo styrene migratory insertion into a Rh–H bond to form **2c**. This migratory insertion transition state (**2-TS2**) has 4 possible styrene conformations. The aryl ring of styrene can reside in the UC, LC, UT, or LT conformations, where U and L are upper and lower (relative to the N–Rh–N plane), C and T are cis and trans (relative to the 5-FP backbone). DFT predicts the **2-TS-LC** conformation to be the most favorable, resulting in a free energy barrier of 16.5 kcal/mol relative to **2**. The LC conformation enables favorable interaction between styrene and the 5-FP ligand, similar to **1a**. In ascending free energy and relative to **2**, the other **2-ts2** barriers for UC, LT, and UT are 17.6, 20.8, and 22.9 kcal/mol, respectively. Again, we see the C conformations to be lower in free energy due to the favorable vdW interactions between styrene and the 5-FP ligand. In **2c**, the H axial to the N–Rh–N plane reorients to reside in the plane; the chloride subsequently binds to Rh via the axial coordination site so that Rh remains 5-coordinate. Finally, the complex overcomes the last barrier (**2-TS3**) in which the second H atom is transferred

leading to reductive elimination of ethylbenzene. The transition state **2-TS3** lies 18.9 kcal/mol above **2**, and the reduced intermediate $[(5\text{-FP})RhCl]^+$ and free ethylbenzene (**2d**) are -5.6 kcal/mol relative to the starting state. Our calculations are consistent with the oxidative addition of dihydrogen (**2-TS1**) being the rate-limiting step; **2-TS3** requires 2.1 kcal/mol less than **2-TS1**.

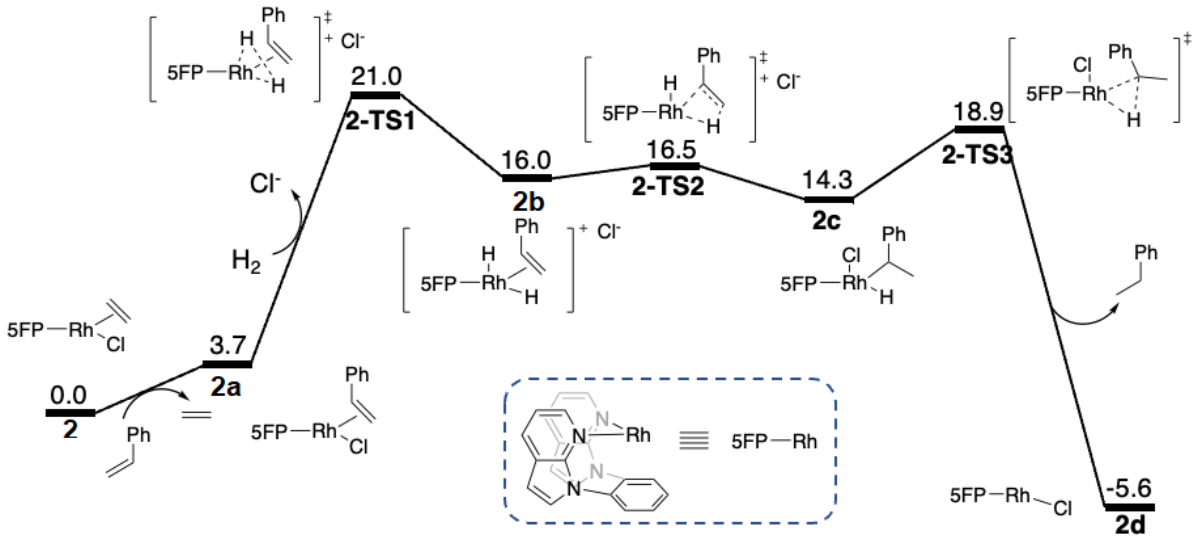

Scheme 8. DFT free energies at 318 K for conversion of styrene to ethyl benzene using (5-FP)Rh(η^2-C_2H_4)Cl (**2**) as catalyst precursor. Free energies are in kcal/mol.

For comparison, we also predicted the Gibbs free energy surface for the catalytic hydrogenation of styrene using **1** as catalyst precursor. Experiments reveal that at 318 K, Rh with the 6-FP ligand produces ethylbenzene nearly twice as fast as Rh with the 5-FP ligand. The complex **2** generates ethylbenzene at a rate of 0.41(4) μM/s while **1** gives a catalytic rate of 0.822(8) μM/s (Figure 1). The rate-limiting oxidative addition barrier for the 5-FP ligand is calculated to be 21.0 kcal/mol (**2-TS1**). We anticipated that the 6-FP ligand might lower the activation barrier and improve the thermodynamics for oxidative addition of dihydrogen since the arene moiety would be positioned closer to the Rh center and consequently favor the Rh(III) product, hence providing a stabilizing effect. The free energy surface for conversion of styrene to ethylbenzene by **1** is displayed below (Scheme 9).

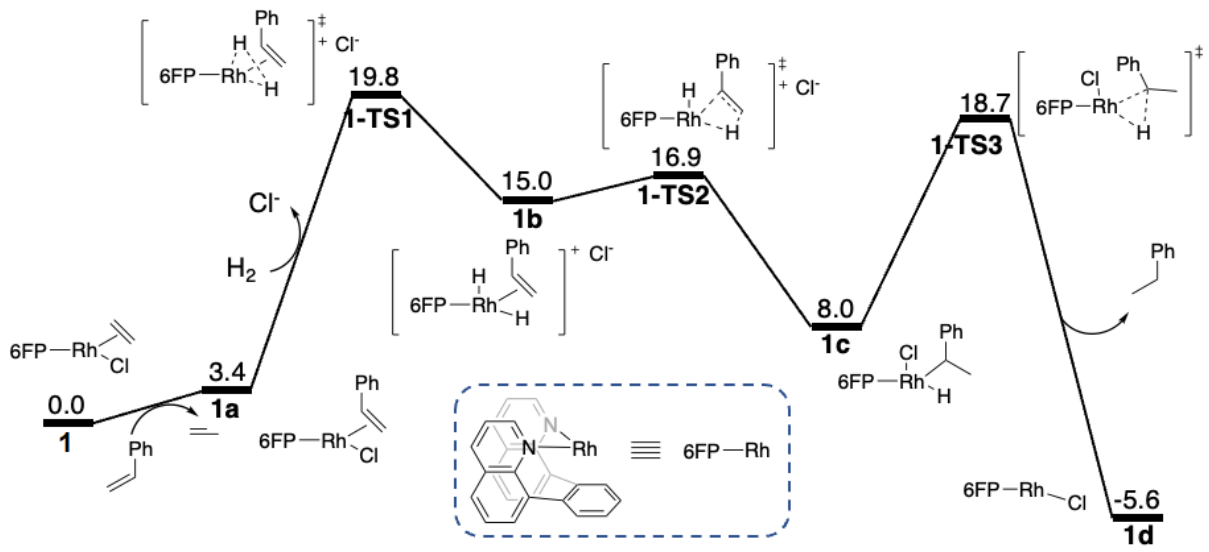

Scheme 9. DFT free energies at 318 K for conversion of styrene to ethyl benzene via the (6-FP)Rh(η^2-C_2H_4)Cl (**1**) catalyst. Free energies are in kcal/mol.

The proposed mechanism based on DFT calculations (Scheme 9) is consistent with the mechanism based on experimental results shown in Scheme 7. Starting with **1** at 0.0 kcal/mol, the displacement of ethylene by styrene is endergonic by 3.4 kcal/mol (**1a**). For **1**, the Rh–C_{cap} distances are calculated to be 2.96 Å and 3.03 Å; for **1a**, these same distances are decreased to 2.91 Å and 3.00 Å. Oxidative addition of H_2 requires a free energy barrier of 19.8 kcal/mol (**1-TS1**), leading to **1b** at 15.0 kcal/mol above the starting state. For subsequent styrene insertion into a Rh–H bond, DFT predicts a barrier of 16.9 kcal/mol (**1-TS2-UC**). For **1-TS2**, the LC, UT, and LT conformers stand 17.3, 19.2, and 20.7 kcal/mol above **1**, such that the UC yields the lowest barrier. Again, the C conformations are lower in energy than the T analogs; however, **1-TS2** prefers structure UC while **2-TS2** prefers LC. This is a consequence of the stacking orientation of styrene with the 5-FP and 6-FP ligands. The following intermediate, (6-FP)Rh(C_8H_9)Cl (**1c**) lies significantly lower than the 5-FP analog at 8.0 kcal/mol relative to **1**. We hypothesize that this lowering in free energy is due to stabilization of the Rh^{III} center by the 6-FP capping arene moiety. Rh^{III} is a saturated 18-electron system that prefers an octahedral coordination environment. The

5-FP ligand prevents Rh^{III} of this preferred 6-coordinate geometry since the arene is positioned at a distance that challenges arene to Rh electron-donation; however, 6-FP allows the Rh^{III} in **1c** to achieve a pseudo-octahedral coordination with a Rh–C_{cap} distance of 2.49 Å, thus making **1c** a low-energy intermediate. In comparison, the analogous Rh–C_{cap} distance in **2c** is 2.74 Å. The trend that a Rh^{III} complex with 6-FP ligand is more stable than the similar Rh^{III} complex with 5-FP ligand is consistent with our previous studies, in which the reductive elimination of (5-FP)Rh(Me)$(TFA)_2$ (TFA = trifluoroacetate) is faster and gives higher yield than (6-FP)Rh(Me)$(TFA)_2$.[35] Finally, reductive elimination to form free ethylbenzene through **1-TS3** is predicted by DFT to be 18.7 kcal/mol above the starting state, leading to (6-FP)RhCl (**1d**) and a free ethylbenzene at -5.6 kcal/mol. Both mechanisms in Scheme 8 and Scheme 9 are different from the proposed mechanism for olefin hydrogenation catalyzed by a Rh complex bearing a hemilabile PNN ligand, which is proposed to follow a "hydrogen first" mechanism involving the release of one coordination site from the hemilabile ligand to allow olefin coordination.[63] In contrast, in our proposed mechanisms the capping arene ligand does not change its coordination number, rather, the position of the arene relative to Rh influences the energetics of intermediates and transition states.

Because TS1 is calculated to be the highest barrier for catalyst precursors with both the 5-FP and 6-FP mechanisms, it is likely the primary contributor to the kinetic rate for styrene hydrogenation. In the calculated pathway using the 5-FP ligand, $\Delta G^{\ddagger}_{5FP}$ for the dihydrogen oxidative addition is 21.0 kcal/mol. For the 6-FP ligand, $\Delta G^{\ddagger}_{6FP}$ is reduced to 19.8 kcal/mol. The calculated $\Delta G^{\ddagger}_{6FP}$ is consistent with the experimental value from the Eyring plot, which is 20(1) kcal/mol (Figure 4).

The difference in barriers for dihydrogen oxidative addition ($\Delta\Delta G^{\ddagger} = \Delta G^{\ddagger}_{6FP} - \Delta G^{\ddagger}_{5FP}$) is -1.2 kcal/mol. Using the Eyring equation along with our computed $\Delta\Delta G^{\ddagger}$, we predict that the 6-FP

ligand enables Rh to produce ethylbenzene 6.6 times faster than 5-FP, which, given deviations in both experimental and computational data, agree well with the experimentally observed rate enhancement of approximately 2-fold for 6-FP over 5-FP. These results are consistent with our hypothesis that 6-FP ligands should favor Rh(III) states more than 5-FP ligands. Our rationalization is that the 6-FP structure places the arene group of the capping arene ligand in closer proximity to Rh(III), hence enhancing arene to Rh donation and providing a more stable complex. In contrast, the 5-FP structure, which positions the arene group farther, should relatively destabilize the Rh(III) state. The calculated Rh–C_{cap} distances in both the transition states for dihydrogen oxidative addition and the products are consistent with this explanation. In **2-TS1** the Rh–C_{cap} distances are 3.04 and 3.28 Å. The analogous distances for **1-TS2** are 2.82 and 3.14 Å (Figure 8). Additionally, the non-covalent interaction of the outer-shell Cl^- with the reacting H_2 seems to play a role. In **2-TS1**, the Cl–H distance is quite short at 1.86 Å (not shown), whereas this distance is increased to 2.05 Å in **1-TS1**, indicating a weaker interaction. Because Cl^- induces a partial positive charge on the H, a stronger interaction means a more positive H, which is less likely to bind to Rh. Indeed, the free energy surfaces show this to be the case. The Cl–H distance in **2-TS1** is shorter by 0.19 Å, resulting in a stronger dipole and thus more positive charge on H, which in turn requires a higher free energy barrier to oxidize Rh.

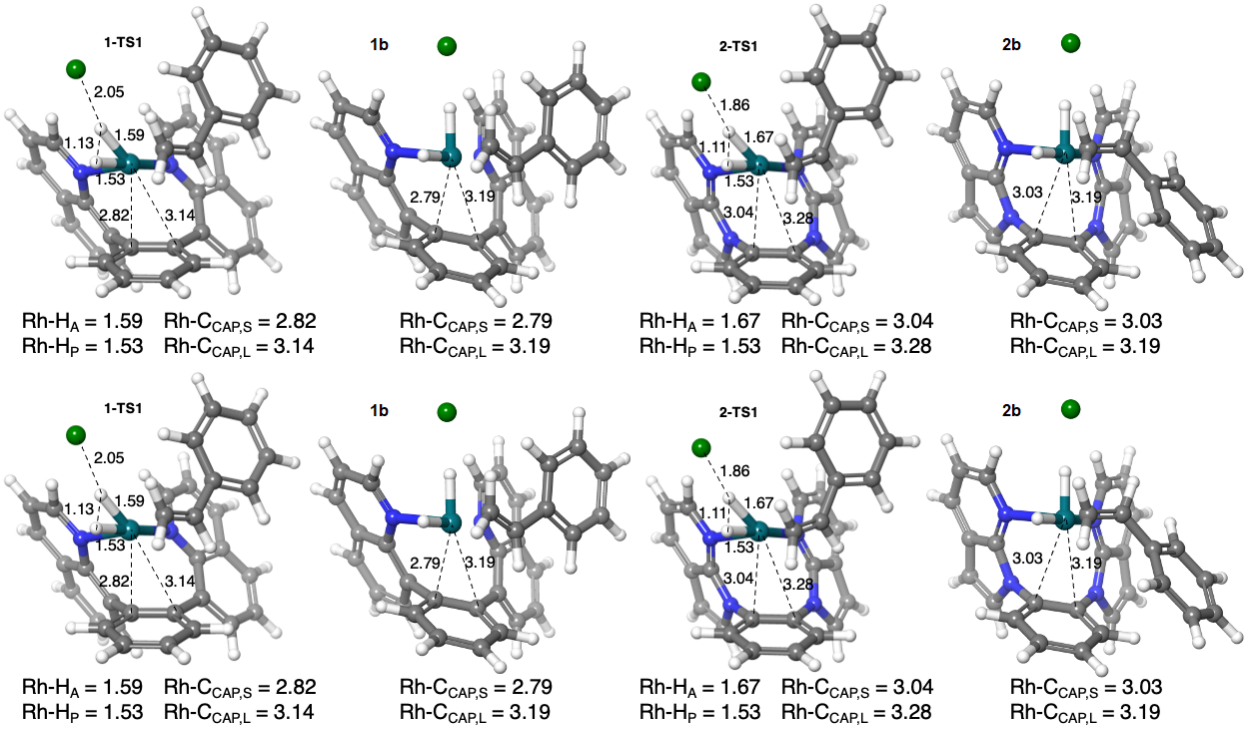

Figure 8. DFT-optimized transition states (**1-TS1** and **2-TS1**) and products (**1b** and **2b**) for H_2 oxidative addition for: (5-FP)Rh(η^2-styrene)Cl (left) and (6-FP)Rh(η^2-styrene)Cl (right). Distances are in Å. Rh-H_A and Rh-H_P denotes distances between Rh and the axial and in-plane hydrogens, respectively. Rh-$C_{CAP,S}$ and Rh-$C_{CAP,L}$ denote the short and long distances between Rh and the 2 closest C's of the arene moieties.

Although the transition states for the reductive elimination of ethylbenzene from **2c** and **1c** show a very close relative energy (~0.2 kcal/mol difference) with respect to the catalyst precursor (**2** or **1**, respectively), the difference between the activation energies for the reductive elimination of **2c** and **1c** is significant. The calculated activation energy for the reductive elimination of **2c** is 4.6 kcal/mol, whereas the activation energy for the reductive elimination of **1c** is 10.7 kcal/mol. This activation barrier difference in reductive elimination could be attributed to the difference in stability of **2c** and **1c**, as discussed above.

Summary and Conclusions

We have investigated the ligand effect of four capping arene-Rh complexes on olefin hydrogenation reactions. The trend on reaction rates indicates an observed dependence on the coordinated capping arene ligand where **4** > **1** > **2**, while the **3** undergoes rapid decomposition process to generate free ligand. Based on the kinetic and computational modeling studies, an "olefin first" hydrogenation mechanism has been proposed. For the comparison of **2** and **1**, the DFT calculations are consistent with our hypothesis. Relative to 5-FP, the structure of the 6-FP ligand stabilizes Rh(III) complexes and the dihydrogen oxidative addition transition state that forms the first Rh(III) intermediate. Our computational modeling suggests that the rate-determining step is probably the oxidative addition of dihydrogen, and the calculated activation barrier for **1** catalyzed styrene hydrogenation is 1.2 kcal/mol lower than that for **2**, which is consistent with our experimental results. We anticipate that the strategy of using the structural features of capping arene ligands, and specifically metal/arene distance and bonding, to modulate the energetics of intermediates and transition states can be extended to other catalytic reactions, especially those that proceed via formal redox and coordination number/geometry changes.

Experimental Section

General Methods. Unless otherwise noted, all reactions were operated under a dinitrogen atmosphere in a glovebox (O_2 < 10 ppm) or using standard Schlenk line techniques. All solvents were dried, degassed and stored in the glovebox with 4Å molecular sieves. All glassware was dried in an oven (150 °C) overnight before use. All NMR spectra were recorded on Varian Inova 600 MHz spectrometer or Bruker Advance III 800 MHz spectrometer. The operating frequency for $^{13}C\{^1H\}$ NMR spectroscopy is 150 MHz (on 600 MHz instrument) or 201 MHz (on 800 MHz instrument). All ^1H NMR and $^{13}C\{^1H\}$ NMR spectra are referenced against the residual ^1H

resonances (^{1}H NMR) or the ^{13}C{^{1}H} resonances (^{13}C{^{1}H} NMR) of the deuterated solvents. All spectra were recorded at 25 °C unless otherwise indicated. The temperature for all variable temperature NMR experiments were calibrated using a MeOH-d_4 standard.[64] The preparation of [Rh(η^2-C_2H_4)$_2$(μ-Cl)]$_2$, 5-FP, 6-FP, 5-^{NP}FP, 6-^{NP}FP, (5-FP)Rh(Cl)(η^2-C_2H_4), (6-FP)Rh(Cl)(η^2-C_2H_4), (5-^{NP}FP)Rh(Cl)(η^2-C_2H_4), (6-^{NP}FP)Rh(Cl)(η^2-C_2H_4) followed reported procedures.[35, 65]

Synthesis and Characterization of (6-FP)Rh(Cl)(*η*^{2}-styrene). To a THF solution (25 mL) of (6-FP)Rh(Cl)(η^2-C_2H_4) (20 mg, 40 μmol), styrene (0.20 mL, 182 mg, 1.75 mmol) was added and stirred at room temperature for 24 hours. The reaction solution was filtered through a Buchner funnel with fine fritted disc. The amount of solvent was reduced by vacuum to obtain a concentrated solution. 30 mL of pentanes was added to the solution, and the products precipitated as an orange powder. X-ray quality crystals of (6-FP)Rh(Cl)(η^2-styrene) were obtained by slow vapor diffusion of *n*-pentane into a benzene solution. Two isomers were obtained with a molecular ratio of approximately 1 (species **A**) to 1.5 (species **B**). ^{1}H NMR (600 MHz, CD_2Cl_2) δ 9.95 (d, *J* = 4 Hz, 1H, Ar–*H*, **A**), 9.85 (d, *J* = 4 Hz, 1H, Ar–*H*, **B**), 8.33 (d, *J* = 4 Hz, 1H, Ar–*H*, **B**), 8.21 (d, *J* = 8 Hz, 1H, Ar–*H*, **A**), 8.13 (d, *J* = 8, 1H, Ar–*H*, **B**), 8.08 (d, *J* = 8 Hz, 1H, Ar–*H*, **B**), 8.05 (d, *J* = 8 Hz, 1H, Ar–*H*, **A**), 7.97 (d, *J* = 7 Hz, 1H, Ar–*H*, **A**), 7.77 (t, *J* = 8 Hz, 1H, Ar–*H*, **B**), 7.73 (t, *J* = 8 Hz, 1H, Ar–*H*, **A**), 7.63 – 7.59 (m, 2H, Ar–*H*, **B**), 7.58 (d, *J* = 7 Hz, 1H, Ar–*H*, **A**), 7.56 – 7.50 (m, 5H), 7.47 – 7.45 (m, 1H, Ar–*H*, **B**), 7.44 (d, *J* = 8 Hz, 2H, Ar–*H*, **B**), 7.43 – 7.39 (m, 2H, Ar–*H*, **A**), 7.32 (t, *J* = 8 Hz, 1H, Ar–*H*, **A**), 7.30 – 7.27 (m, 1H, Ar–*H*, **A**; 1H, Ar–*H*, **B**), 6.98 (t, *J* = 8 Hz, 1H, Ar–*H*, **A**), 6.96 – 6.93 (m, 1H, Ar–*H*, **A**; 1H, Ar–H, **B**), 6.87 (dd, *J* = 7 Hz, 1H, Ar–*H*, **A**), 6.82 (d, *J* = 5 Hz, 1H, Ar–*H*, **A**), 6.76 – 6.69 (m, 4H), 6.45 (t, *J* = 7 Hz, 1H, Ar–*H*, **B**), 6.31 (t, *J* = 7 Hz, 2H, Ar–*H*, **B**), 6.25 (d, *J* = 7 Hz, 2H, Ar–*H*, **B**), 5.88 (dd, *J* = 8, 5 Hz, 1H, **A**), 5.46 – 5.40 (m, 1H, PhC*H*=C, **A**), 3.99 (d, $^{3}J_{HH}$ = 8 Hz, 1H, PhC=C–*H*, **B**), 3.68 (t, $^{3}J_{HH}$ = 10 Hz, 1H, PhC*H*=C, **B**), 2.92 (d, $^{3}J_{HH}$ = 11 Hz, 1H, PhC=C–*H*, **B**), 2.12 (d, $^{3}J_{HH}$ = 12 Hz, 1H, PhC=C–*H*, **A**), 1.73 (d, $^{3}J_{HH}$ = 8 Hz, 1H, PhC=C–*H*, **A**). ^{13}C NMR (201 MHz, CD_2Cl_2) δ 156.6, 154.3, 154.1, 153.9, 151.1, 150.2,

150.2, 147.0, 146.8, 141.3, 141.2, 140.7, 140.6, 138.1, 137.4, 136.9, 136.8, 135.5, 135.1, 134.9, 134.6, 133.9, 133.4, 132.8, 132.5, 131.5, 131.4, 131.2, 130.2, 127.8, 127.6, 127.5, 127.4, 127.2, 127.1, 126.9, 126.8, 126.7, 126.4, 126.3, 124.4, 124.1, 122.4, 122.2, 121.8, 121.5, 120.5, 114.1, 57.8 (d, $^1J_{Rh-C}$ = 18 Hz, Ph–*C* for coordinated styrene on **A**), 48.2 (d, $^1J_{Rh-C}$ = 13 Hz, Ph–*C* for coordinated styrene on **B**), 41.6 (d, $^1J_{Rh-C}$ = 21 Hz, PhC=*C* for coordinated styrene on **B**), 33.5 (d, $^1J_{Rh-C}$ = 13 Hz, PhC=*C* for coordinated styrene on **A**). We were unable to obtain satisfactory elemental analysis since the complex decomposes under vacuum.

Kinetic studies for (6-FP)Rh(Cl)(η^2-C_2H_4) catalyzed styrene hydrogenation. In a glovebox with nitrogen atmosphere, 0.40 mL of stock solution in CD_2Cl_2 with (6-FP)Rh(Cl)(η^2-C_2H_4), styrene and HMB (internal standard) was added to a J. Young tube, followed by charging dihydrogen gas. The concentration or pressure of the added chemicals is noted in Figure *2*. The J. Young tube was heated to 45 °C in the NMR instrument. Arrayed ^{1}H NMR spectra were obtained for the initial rates of the styrene hydrogenation.

Eyring plots for (6-FP)Rh(Cl)(η^2-C_2H_4) catalyzed styrene hydrogenation. The sample preparation is similar to the kinetic studies described above. A J. Young tube was loaded with 0.40 mL of stock solution in CD_2Cl_2 containing 1 mM (6-FP)Rh(Cl)(η^2-C_2H_4), 44 mM styrene and 0.6 mM HMB (internal standard) under N_2 atmosphere, and then pressurized with 50 psig H_2. The J. Young tube was heated to the designated temperature noted in Figure 4 in the NMR instrument. Arrayed ^{1}H NMR spectra were obtained to measure the initial rates of the styrene hydrogenation.

Isotopic study for (6-FP)Rh(Cl)(η^2-C_2H_4) catalyzed styrene hydrogenation. In a J. Young tube, 8 mg (0.016 mmol) (6-FP)Rh(Cl)(η^2-C_2H_4) and 10 μL (9.1 mg, 0.087 mmol) styrene were added and dissolved in 0.5 mL CD_2Cl_2 under N_2 atmosphere. The tube was charged with 50 psig of D_2, and heated to 40 °C in an oil bath. The reaction was monitored by ^{1}H NMR every 24 hours.

Computational Methods. All Density Functional Theory calculations were performed using the Jaguar v10.9 software package by Schrödinger Inc.[66] All calculations utilized the B3LYP hybrid functional[67, 68] but including the Grimme-Becke-Jonson D3 correction for London dispersion forces.[69] Rh atoms were described using the Los Alamos large-core pseudopotential (9 explicit electrons)[70, 71] augmented with diffuse and polarization functions. All other atoms were described by the 6-311G**++ basis set, including polarization and diffuse functions (designated LAV3P**++ in Jaguar). All calculations also included implicit solvent as described by the PBF Poisson Boltzmann continuum model.[72, 73] We use solvent parameters of: dielectric constant = 8.93 and probe radius = 2.33 Å to match dichloromethane.

Following geometry optimizations, we performed frequency calculations. These calculations served to confirm the intermediate states (no negative eigenmodes in the Hessian) and transition states (single negative eigenmodes in the Hessian). Frequency calculations also served to predict the thermochemical properties (enthalpies, entropies, and free energies) at 318 K.

We also performed periodic calculations using the VASP Software.[74] These calculations utilized the PBE GGA functional[75] with the Grimme-Becke-Johnson D3 correction for London dispersion. PAW pseudopotentials were used for all atoms. The plane-wave basis set cutoff was set to 500 eV. Implicit solvent via the VASPsol[76, 77] module was used with a dielectric constant = 8.93.

Crystallographic Details. A crystal of **1a** or **4a** was coated with Paratone oil and mounted on a MiTeGen MicroLoop. The X-ray intensity data were measured on a Bruker D8 Venture Photon III Kappa four-circle diffractometer system equipped with Incoatec IμS 3.0 micro-focus sealed X-ray tubes (Mo Kα, λ = 0.71073 Å; Cu Kα, λ = 1.54178 Å) and HELIOS double bounce multilayer mirror monochromators. The frames were integrated with the Bruker SAINT software package[78] using a narrow-frame algorithm. Data were corrected for absorption effects using the

Multi-Scan method (SADABS).[78] The structure was solved and refined using the Bruker SHELXTL Software Package[79] within APEX3/4 [78] and OLEX2[80]. Non-hydrogen atoms were refined anisotropically. The vinylic hydrogen atoms on C25 and C26 in **4a** were located in the electron density map and refined isotropically. All other hydrogen atoms in both structures were placed in geometrically calculated positions with U_{iso} = 1.2U_{equiv} of the parent atom. In **1a**, each solvent site and part of the main molecule were disordered over two positions. The relative occupancy at each site was freely refined. Constraints and restraints were used on the anisotropic displacement parameters and bond lengths of most of the disordered atoms. CCDC 2166578 and 2201532 contains the supplementary crystallographic data for this paper.

Supporting Information

Additional experimental details, kinetic plots, crystal structure details and details of computational studies, including x, y and z coordinates.

Acknowledgements. Experimental work was supported by the U.S. National Science Foundation under award CHE-2102433 with financial support for purchase of an X-ray diffractometer provided by CHE-2018870. CBM and WAG were supported by Office of Naval Research (ONR) under award N00014-19-1-2081.

Dedication. We are pleased to have the opportunity to contribute to this special issue in celebration of Maurice Brookhart's remarkable career. Brooks' research and teaching innovated significant insights and fundamental advancements and positively impacted the careers and lives of all those who had the pleasure to work with him.

Author Information

Corresponding Authors

William A. Goddard III - *Materials and Process Simulation Center, California Institute of Technology, Pasadena, CA 91125, United States;* orcid.org/0000-0003-0097-5716; Email: wag@caltech.edu

T. Brent Gunnoe - *Department of Chemistry, University of Virginia, Charlottesville, VA 22904, United State;* orcid.org/0000-0001-5714-3887; Email: tbg7h@virginia.edu

Authors

Ke Zhang - *Department of Chemistry, University of Virginia, Charlottesville, VA 22904, United State;* orcid.org/0000-0001-8090-7179

Charles B. Musgrave III - *Materials and Process Simulation Center, California Institute of Technology, Pasadena, CA 91125, United States;* orcid.org/0000-0002-3432-0817

Diane A. Dickie - *Department of Chemistry, University of Virginia, Charlottesville, VA 22904, United State;* orcid.org/0000-0003-0939-3309

Author Contributions

[#] K.Z. and C.M. contributed equally to this work.

Notes

The authors declare no competing financial interests.

References

(1) Hartwig, J. F. *Organotransition Metal Chemistry: From Bonding to Catalysis*; University Science book, 2009.

(2) Crabtree, R. H. *Oxidative Addition and Reductive Elimination*; 2014.

(3) Biffis, A.; Centomo, P.; Del Zotto, A.; Zecca, M. Pd Metal Catalysts for Cross-Couplings and Related Reactions in the 21st Century: A Critical Review. *Chem. Rev.* **2018**, *118*, 2249-2295.

(4) Chinchilla, R.; Nájera, C. Recent advances in Sonogashira reactions. *Chem. Soc. Rev.* **2011**, *40*, 5084-5121.

(5) Schmidt, A. F.; Kurokhtina, A. A. Distinguishing between the homogeneous and heterogeneous mechanisms of catalysis in the Mizoroki-Heck and Suzuki-Miyaura reactions: Problems and prospects. *Kinet. Catal.* **2012**, *53*, 714-730.

(6) Esteruelas, M. A.; Oro, L. A. Dihydrogen Complexes as Homogeneous Reduction Catalysts. *Chem. Rev.* **1998**, *98*, 577-588.

(7) Sunley, G. J.; Watson, D. J. High productivity methanol carbonylation catalysis using iridium: The Cativa™ process for the manufacture of acetic acid. *Catal. Today* **2000**, *58*, 293-307.

(8) Hjortkjaer, J.; Jensen, V. W. Rhodium Complex Catalyzed Methanol Carbonylation. *Product R&D* **1976**, *15*, 46-49.

(9) Paulik, F. E.; Roth, J. F. Novel catalysts for the low-pressure carbonylation of methanol to acetic acid. *Chem. Commun.* **1968**, 1578a-1578a.

(10) Miyaura, N.; Suzuki, A. Palladium-Catalyzed Cross-Coupling Reactions of Organoboron Compounds. *Chem. Rev.* **1995**, *95*, 2457-2483.

(11) Maitlis, P. M.; Haynes, A.; Sunley, G. J.; Howard, M. J. Methanol carbonylation revisited: thirty years on *Dalton Trans.* **1996**, 2187-2196.

(12) Forster, D. Mechanistic Pathways in the Catalytic Carbonylation of Methanol by Rhodium and Iridium Complexes. In *Adv. Organomet. Chem.*, Stone, F. G. A., West, R. Eds.; Vol. 17; Academic Press, 1979; pp 255-267.

(13) Kalck, P.; Le Berre, C.; Serp, P. Recent advances in the methanol carbonylation reaction into acetic acid. *Coord. Chem. Rev.* **2020**, *402*, 213078.

(14) Heck, R. F.; Breslow, D. S. The Reaction of Cobalt Hydrotetracarbonyl with Olefins. *J. Am. Chem. Soc.* **1961**, *83*, 4023-4027.

(15) Evans, D.; Osborn, J. A.; Wilkinson, G. Hydroformylation of alkenes by use of rhodium complex catalysts. *J. Chem. Soc. A* **1968**, 3133-3142.

(16) Birch, A. J.; Williamson, D. H. Homogeneous Hydrogenation Catalysts in Organic Synthesis. *Org. React.* **2011**, 1-186.

(17) Halpern, J.; Okamoto, T.; Zakhariev, A. Mechanism of the chlorotris(triphenylphosphine) rhodium(I)-catalyzed hydrogenation of alkenes. The reaction of chlorodihydridotris(triphenyl-phosphine)rhodium(III) with cyclohexene. *J. Mol. Catal.* **1977**, *2*, 65-68.

(18) Roseblade, S. J.; Pfaltz, A. Iridium-Catalyzed Asymmetric Hydrogenation of Olefins. *Acc. Chem. Res.* **2007**, *40*, 1402-1411.

(19) Schrock, R. R.; Osborn, J. A. Catalytic hydrogenation using cationic rhodium complexes. II. The selective hydrogenation of alkynes to cis olefins. *J. Am. Chem. Soc.* **1976**, *98*, 2143-2147.

(20) Niu, S.; Hall, M. B. Theoretical Studies on Reactions of Transition-Metal Complexes. *Chem. Rev.* **2000**, *100*, 353-406.

(21) Thompson, W. H.; Sears, C. T. Kinetics of oxidative addition to iridium(I) complexes. *Inorg. Chem.* **1977**, *16*, 769-774.

(22) Kubota, M.; Kiefer, G. W.; Ishikawa, R. M.; Bencala, K. E. Kinetics of reactions of methyl iodide with four-coordinated iridium(I) complexes. *Inorg. Chim. Acta* **1973**, *7*, 195-202.

(23) Gu, S.; Nielsen, R. J.; Taylor, K. H.; Fortman, G. C.; Chen, J.; Dickie, D. A.; Goddard, W. A.; Gunnoe, T. B. Use of Ligand Steric Properties to Control the Thermodynamics and Kinetics of Oxidative Addition and Reductive Elimination with Pincer-Ligated Rh Complexes. *Organometallics* **2020**, *39*, 1917-1933.

(24) Feller, M.; Iron, M. A.; Shimon, L. J. W.; Diskin-Posner, Y.; Leitus, G.; Milstein, D. Competitive C−I versus C−CN Reductive Elimination from a RhIII Complex. Selectivity is Controlled by the Solvent. *J. Am. Chem. Soc.* **2008**, *130*, 14374-14375.

(25) Feller, M.; Diskin-Posner, Y.; Leitus, G.; Shimon, L. J. W.; Milstein, D. Direct Observation of Reductive Elimination of MeX (X = Cl, Br, I) from RhIII Complexes: Mechanistic Insight and the Importance of Sterics. *J. Am. Chem. Soc.* **2013**, *135*, 11040-11047.

(26) O'Reilly, M. E.; Pahls, D. R.; Webb, J. R.; Boaz, N. C.; Majumdar, S.; Hoff, C. D.; Groves, J. T.; Cundari, T. R.; Gunnoe, T. B. Reductive functionalization of a rhodium(III)–methyl bond by electronic modification of the supporting ligand. *Dalton Trans.* **2014**, *43*, 8273-8281.

(27) O'Reilly, M. E.; Fu, R.; Nielsen, R. J.; Sabat, M.; Goddard, W. A.; Gunnoe, T. B. Long-Range C–H Bond Activation by Rh^{III}-Carboxylates. *J. Am. Chem. Soc.* **2014**, *136*, 14690-14693.

(28) Albrecht, M.; van Koten, G. Platinum Group Organometallics Based on "Pincer" Complexes: Sensors, Switches, and Catalysts. *Angew. Chem. Int. Ed.* **2001**, *40*, 3750-3781.

(29) Choi, J.; MacArthur, A. H. R.; Brookhart, M.; Goldman, A. S. Dehydrogenation and Related Reactions Catalyzed by Iridium Pincer Complexes. *Chem. Rev.* **2011**, *111*, 1761-1779.

(30) Goldberg, J. M.; Wong, G. W.; Brastow, K. E.; Kaminsky, W.; Goldberg, K. I.; Heinekey, D. M. The Importance of Steric Factors in Iridium Pincer Complexes. *Organometallics* **2015**, *34*, 753-762.

(31) Goldberg, J. M.; Cherry, S. D. T.; Guard, L. M.; Kaminsky, W.; Goldberg, K. I.; Heinekey, D. M. Hydrogen Addition to (pincer)Ir^{I}(CO) Complexes: The Importance of Steric and Electronic Factors. *Organometallics* **2016**, *35*, 3546-3556.

(32) Frech, C. M.; Milstein, D. Direct Observation of Reductive Elimination of Methyl Iodide from a Rhodium(III) Pincer Complex: The Importance of Sterics. *J. Am. Chem. Soc.* **2006**, *128*, 12434-12435.

(33) Shaffer, D. W.; Ryken, S. A.; Zarkesh, R. A.; Heyduk, A. F. Ligand Effects on the Oxidative Addition of Halogens to (dpp-nacnac^{R})Rh(phdi). *Inorg. Chem.* **2012**, *51*, 12122-12131.

(34) Donoghue, P. J.; Helquist, P.; Wiest, O. Ligand and Substrate Effects on the Mechanism of Rhodium-Catalyzed Hydrogenation of Enamides. *J. Org. Chem.* **2007**, *72*, 839-847.

(35) Gu, S.; Chen, J.; Musgrave, C. B.; Gehman, Z. M.; Habgood, L. G.; Jia, X.; Dickie, D. A.; Goddard, W. A.; Gunnoe, T. B. Functionalization of RhIII–Me Bonds: Use of “Capping Arene” Ligands to Facilitate Me–X Reductive Elimination. *Organometallics* **2021**, *40*, 1889-1906.

(36) O’Reilly, M. E.; Johnson, S. I.; Nielsen, R. J.; Goddard, W. A.; Gunnoe, T. B. Transition-Metal-Mediated Nucleophilic Aromatic Substitution with Acids. *Organometallics* **2016**, *35*, 2053-2056.

(37) Fu, R.; O'Reilly, M. E.; Nielsen, R. J.; Goddard Iii , W. A.; Gunnoe, T. B. Rhodium Bis(quinolinyl)benzene Complexes for Methane Activation and Functionalization. *Eur. J. Chem.* **2015**, *21*, 1286-1293.

(38) Gu, S.; Musgrave, C. B.; Gehman, Z. M.; Zhang, K.; Dickie, D. A.; Goddard, W. A.; Gunnoe, T. B. Rhodium and Iridium Complexes Bearing “Capping Arene” Ligands: Synthesis and Characterization. *Organometallics* **2021**, *40*, 2808–2825.

(39) Liu, C.; Geer, A. M.; Webber, C.; Musgrave, C. B.; Gu, S.; Johnson, G.; Dickie, D. A.; Chabbra, S.; Schnegg, A.; Zhou, H.; et al. Immobilization of “Capping Arene” Cobalt(II) Complexes on Ordered Mesoporous Carbon for Electrocatalytic Water Oxidation. *ACS Catal.* **2021**, *11*, 15068-15082.

(40) Chen, J.; Nielsen, R. J.; Goddard, W. A.; McKeown, B. A.; Dickie, D. A.; Gunnoe, T. B. Catalytic Synthesis of Superlinear Alkenyl Arenes Using a Rh(I) Catalyst Supported by a “Capping Arene” Ligand: Access to Aerobic Catalysis. *J. Am. Chem. Soc.* **2018**, *140*, 17007-17018.

(41) Chan, A. S. C.; Halpern, J. Interception and characterization of a hydridoalkylrhodium intermediate in a homogeneous catalytic hydrogenation reaction. *J. Am. Chem. Soc.* **1980**, *102*, 838-840.

(42) Halpern, J. Mechanism and Stereoselectivity of Asymmetric Hydrogenation. *Science* **1982**, *217*, 401-407.

(43) Yuan, X.; Bi, S.; Ding, Y.; Liu, L.; Sun, M. DFT study of alkene hydrogenation catalyzed by $Rh(acac)(CO)_2$. *J. Organomet. Chem.* **2010**, *695*, 1576-1582.

(44) Imamoto, T.; Tamura, K.; Zhang, Z.; Horiuchi, Y.; Sugiya, M.; Yoshida, K.; Yanagisawa, A.; Gridnev, I. D. Rigid P-Chiral Phosphine Ligands with tert-Butylmethylphosphino Groups for Rhodium-Catalyzed Asymmetric Hydrogenation of Functionalized Alkenes. *J. Am. Chem. Soc.* **2012**, *134*, 1754-1769.

(45) Meakin, P.; Jesson, J. P.; Tolman, C. A. Nature of chlorotris(triphenylphosphine)rhodium in solution and its reaction with hydrogen. *J. Am. Chem. Soc.* **1972**, *94*, 3240-3242.

(46) Ke, Z.; Li, Y.; Hou, C.; Liu, Y. Homogeneously catalyzed hydrogenation and dehydrogenation reactions – From a mechanistic point of view. *Phys. Sci. Rev.* **2018**, *3*, 20170038.

(47) Luo, J.; Oliver, A. G.; Scott McIndoe, J. A detailed kinetic analysis of rhodium-catalyzed alkyne hydrogenation. *Dalton Trans.* **2013**, *42*, 11312-11318.

(48) Guo, X.; Scott, P. J.; Rempel, G. L. Catalytic hydrogenation of diene polymers: Part II. Kinetic analysis and mechanistic studies on the hydrogenation of styrene—butadiene copolymers in the presence of $RhCl(PPh_3)_3$. *J. Mol. Catal.* **1992**, *72*, 193-208.

(49) Ungváry, F. Transition metals in organic synthesis: Hydroformylation, reduction, and oxidation. Annual survey covering the year 1992. *J. Organomet. Chem.* **1994**, *477*, 363-430.

(50) Straub, B. F. Organotransition Metal Chemistry. From Bonding to Catalysis. Edited by John F. Hartwig. *Angew. Chem. Int. Ed.* **2010**, *49*, 7622-7622.

(51) Srinivasan, B. Words of Advice: teaching enzyme kinetics. *The FEBS Journal* **2021**, *288*, 2068-2083.

(52) Jeske, G.; Lauke, H.; Mauermann, H.; Schumann, H.; Marks, T. J. Highly reactive organolanthanides. A mechanistic study of catalytic olefin hydrogenation by bis(pentamethylcyclopentadienyl) and related 4f complexes. *J. Am. Chem. Soc.* **1985**, *107*, 8111-8118.

(53) Vazquez-Serrano, L. D. Catalytic homogeneous hydrogenation of olefins using N-heterocyclic carbene complexes of rhodium and iridium. Ph.D. Dissertation, Purdue University, Ann Arbor, MI., 2004.

(54) Jardine, F. H.; Osbron, J. A.; Wilkinson, G. Further studies on the homogeneous hydrogenation of olefins using tris(triphenylphosphine)halogenorhodium(I) catalysts. *J. Chem. Soc. A* **1967**, 1574-1578.

(55) Chatt, J.; Venanzi, L. M. Olefin Complexes of Rhodium. *Nature* **1956**, *177*, 852-853.

(56) Albright, T. A. H., R.; Thibeault, J.C.; Thorn, D.L. Ethylene Complexes. Bonding, Rotational Barriers, and Conformational Preferences. *J. Am. Chem. Soc.* **1979**, *101*, 3801-3812.

(57) Cramer, R. Olefin Coordination Compounds of Rhodium: The Barrier to Rotation of Coordinated Ethylene and the Mechanism of Olefin Exchange. *J. Am. Chem. Soc.* **1964**, *86*, 217-222.

(58) Kaneshima, T.; Yumoto, Y.; Kawakami, K.; Tanaka, T. Rotation of olefins in dithiocarbamatobis(isocyanide)(olefin)rhodium complexes. *Inorg. Chim. Acta* **1976**, *18*, 29-34.

(59) Bodner, G. S. F., J. M.; Arif, A. M.; Gladysz, J. A. Selective Binding of One Enantioface of Monosubstituted Alkenes to the Chiral Transition Metal Lewis Acid $[(\eta^5\text{-}C_5H_5)Re(NO)(PPh_3)]^+$. *J. Am. Chem. Soc.* **1988**, 4082-4084.

(60) Valahovic, M. T.; Gunnoe, T. B.; Sabat, M.; Harman, W. D. Ligand-Modulated Stereo- and Regioselective Tandem Addition Reactions of Rhenium-Bound Naphthalene. *J. Am. Chem. Soc.* **2002**, *124*, 3309-3315.

(61) Brooks, B. C.; Meiere, S. H.; Friedman, L. A.; Carrig, E. H.; Gunnoe, T. B.; Harman, W. D. Interfacial and Intrafacial Linkage Isomerizations of Rhenium Complexes with Aromatic Molecules. *J. Am. Chem. Soc.* **2001**, *123*, 3541-3550.

(62) Larpent, C.; Patin, H. Mechanistic aspects of alkenes hydrogenation and deuteration catalyzed by dispersion of hydroxyhydridorhodium colloids in aqueous medium. *J. Mol. Catal.* **1990**, *61*, 65-73.

(63) Masson, J.-P.; Bahsoun, A. A.; Youinou, M.-T.; Osborn, J. A. 'A rendezvous with an old flame': revisiting olefin hydrogenation with new rhodium and iridium catalysts. *Comptes Rendus Chimie* **2002**, *5*, 303-308.

(64) Findeisen, M.; Brand, T.; Berger, S. A ^{1}H-NMR thermometer suitable for cryoprobes. *Magn. Reson. Chem.* **2007**, *45*, 175-178.

(65) Zhao, S.-B.; Song, D.; Jia, W.-L.; Wang, S. Regioselective C−H Activation of Toluene with a 1,2-Bis(N-7-azaindolyl)benzene Platinum(II) Complex. *Organometallics* **2005**, *24*, 3290-3296.

(66) Bochevarov, A. D.; Harder, E.; Hughes, T. F.; Greenwood, J. R.; Braden, D. A.; Philipp, D. M.; Rinaldo, D.; Halls, M. D.; Zhang, J.; Friesner, R. A. Jaguar: A high-performance quantum chemistry software program with strengths in life and materials sciences. *Int. J. Quantum Chem* **2013**, *113*, 2110-2142.

(67) Becke, A. D. Density-functional thermochemistry. III. The role of exact exchange. *J. Chem. Phys.* **1993**, *98*, 5648-5652.

(68) Lee, C.; Yang, W.; Parr, R. G. Development of the Colle-Salvetti correlation-energy formula into a functional of the electron density. *Phys. Rev. B* **1988**, *37*, 785-789.

(69) Grimme, S.; Antony, J.; Ehrlich, S.; Krieg, H. A consistent and accurate ab initio parametrization of density functional dispersion correction (DFT-D) for the 94 elements H-Pu. *J. Chem. Phys.* **2010**, *132*, 154104.

(70) Kahn, L. R.; Goddard, W. A. Ab Initio Effective Potentials for Use in Molecular Calculations. *J. Chem. Phys.* **1972**, *56*, 2685-2701.

(71) Roy, L. E.; Hay, P. J.; Martin, R. L. Revised Basis Sets for the LANL Effective Core Potentials. *J. Chem. Theory Comput.* **2008**, *4*, 1029-1031.

(72) Friedrichs, M.; Zhou, R.; Edinger, S. R.; Friesner, R. A. Poisson−Boltzmann Analytical Gradients for Molecular Modeling Calculations. *J. Phys. Chem. B* **1999**, *103*, 3057-3061.

(73) Tannor, D. J.; Marten, B.; Murphy, R.; Friesner, R. A.; Sitkoff, D.; Nicholls, A.; Honig, B.; Ringnalda, M.; Goddard, W. A. Accurate First Principles Calculation of Molecular Charge Distributions and Solvation Energies from Ab Initio Quantum Mechanics and Continuum Dielectric Theory. *J. Am. Chem. Soc.* **1994**, *116*, 11875-11882.

(74) Hafner, J. Ab-initio simulations of materials using VASP: Density-functional theory and beyond. *J. Comput. Chem.* **2008**, *29*, 2044-2078.

(75) Perdew, J. P.; Burke, K.; Ernzerhof, M. Generalized Gradient Approximation Made Simple. *Phys. Rev. Lett.* **1996**, *77*, 3865-3868.

(76) Mathew, K.; Sundararaman, R.; Letchworth-Weaver, K.; Arias, T. A.; Hennig, R. G. Implicit solvation model for density-functional study of nanocrystal surfaces and reaction pathways. *J. Chem. Phys.* **2014**, *140*, 084106.

(77) Mathew, K.; Kolluru, V. S. C.; Mula, S.; Steinmann, S. N.; Hennig, R. G. Implicit self-consistent electrolyte model in plane-wave density-functional theory. *J. Chem. Phys.* **2019**, *151*, 234101.

(78) *Saint; SADABS; APEX3*; Bruker AXS Inc.: Madison, Wisconsin, USA., 2012. (accessed 2022).

(79) Sheldrick, G. SHELXT - Integrated space-group and crystal-structure determination. *Acta Crystallogr. A* **2015**, *71*, 3-8.

(80) Dolomanov, O. V.; Bourhis, L. J.; Gildea, R. J.; Howard, J. A. K.; Puschmann, H. OLEX2: a complete structure solution, refinement and analysis program. *J. Appl. Crystallogr.* **2009**, *42*, 339-341.

Table of Contents Graphic